

# Thermodynamic behaviour of magnetocaloric quantities in spin-1/2 Ising square trilayer

Soham Chandra<sup>†</sup> and Muktish Acharyya<sup>\*</sup>  
 Department of Physics, Presidency University  
 86/1 College Street, Calcutta-700073, India

E-mail: <sup>†</sup>soham.rs@presiuniv.ac.in; <sup>\*</sup>muktish.physics@presiuniv.ac.in

## Abstract

We have studied a quasi three-dimensional, spin-1/2, Ising trilayer magnetic system on square Bravais lattice, employing Monte-Carlo simulation with single spin-flip Metropolis algorithm. The bulk of such a system is formed by three alternate layers, each of which is composed completely either of A or B type of atoms, resulting in two distinct compositions: ABA and AAB. The interactions between like atoms is ferromagnetic and between unlike ones, is anti-ferromagnetic. Variation of relative interaction strengths in the Hamiltonian, for a range of values, leads to the shift of compensation point and critical point and changes in the magnitude of reduced residual magnetisation. We have tried to put forward probable mathematical forms of dependence for the reduced residual magnetisation and temperature interval between the compensation and critical points on controlling parameters in absence of applied magnetic field and have obtained phase diagrams for both types of configurations from these relations.

**Keywords:** Ising trilayer, Metropolis algorithm, residual magnetisation, compensation temperature, critical temperature

## I. Introduction

After the discovery of the *magnetocaloric effect* (MCE) in iron by Warburg in 1881 [1], theoretical explanations were provided by Debye in 1926 [2] and Giauque in 1927 [3]. MCE is defined by heating or cooling of a magnetic material, with the variation of applied magnetic field and it is a good candidate for cryogenics and construction of energy efficient devices and that is why its potential is investigated [4-7]. We have a few exactly solvable spin-models like Jordan-Wigner transformation [8] and Bethe ansatz-based quantum transfer matrix and nonlinear integral equations method [9], dealing with various magneto-caloric quantities. Recent analytical approaches [10-16] mostly use mean field approximation to develop scaling-based equations of state for the thermodynamics of magnetic systems. Numerical studies e.g. Monte Carlo (MC) simulations [17,18] are widely used to predict the magneto-caloric properties of promising materials [19-21] for MCE.

Our area of interest in this article is compensation points which is a very exciting property of layered ferrimagnets. Compensation point,  $T_{comp}$ , is that temperature, below the antiferromagnetic critical temperature or the Néel temperature where the total magnetization of the bulk becomes zero, though we still observe non-zero sublattice magnetization. It is reported, by Mean field approximation and Effective Field approximation [22] and by MC simulations with Single cluster Wolff Algorithm [23] that under certain range of different types of interaction strengths between lattice sites, different temperature dependencies of sublattice magnetisations cause the compensation point to appear in an Ising trilayer on square lattice. This compensation phenomenon is not related to critical phenomena but some physical properties like the magnetic coercivity of the system may exhibit a singular behavior at the compensation point [24-26]. In [26] the authors have reported some ferrimagnets have their compensation points near room temperature which makes them ideal candidates for magneto-optical drives. A quasi three-dimensional, spin-1/2, Ising trilayer stacking on square lattice with quenched non-magnetic impurity is studied in [27] and it is observed, the critical (each of all sublattice magnetisations vanish) and compensation points (total magnetisation vanishes for nonzero sublattice magnetisations), can be modulated to drift towards lower temperatures with increasing concentration of non-magnetic impurities and in [28], it was hinted that reduced residual magnetisation, another magnetocaloric quantity, possibly varies in a systematic way, which needs further attention.

MCE can be conveniently used for cooling a sample and may offer larger efficiencies than conventional refrigeration processes. To make magnetic cooling economically more affordable, we need to design a material which will have total magnetisation zero at a low enough temperature so that lesser numbers of isothermal magnetization and adiabatic demagnetization is needed to be performed to reach microkelvin order and that particular temperature should ideally be controlled by fewer number of controlling parameters. For such systems, compensation temperature can be that desired low enough temperature with total magnetisation equal to zero which is much below than the critical temperature of the system. The point to be further investigated is if we can shift the compensation temperature towards lower values by controlling parameters namely relative interaction strengths. We have already introduced compensation temperature in Introduction. Next we wish to introduce Reduced residual magnetisation as the absolute value of the ratio of the peak value of the magnetisation in between Néel and compensation points and the saturated value of magnetisation and observe its variation with controlling parameters. These final two observations might be helpful for experimentalists in designing a material for their desired purposes.

Referring to recent studies on layered magnetism in the literature, experimental realisation of the layered magnetic

materials e.g. bilayer [29], trilayer [30,31] and multilayer [32-35] is reported. In [36], the dilution effects on compensation temperature in nanotrilinear graphene structure were studied through MC simulation and it has been found that with reduction in dilution probability, compensation temperature, *increases* in an ABA system and *decreases* in BAB systems. In [37], by the MC approach, the appearance of two compensation temperatures is reported in a mixed spin (7/2, 1) antiferromagnetic ovalene nanostructures. It was observed by MC simulation [38], in Blume Capel model of a bilayer graphene structure with Ruderman-Kittel-Kasuya-Yosida (RKKY) interactions, the transition temperature increases with decrease in the number of nonmagnetic layers. The trilayered Blume-Capel ( $S = 1$ ) magnet is studied in [39] by Monte Carlo simulation and the equilibrium behaviours of critical and compensation temperatures and the dependence of these two temperature on the anisotropy are reported and comprehensive phase diagrams in Hamiltonian parameter space are drawn.

The formation of this article is as follows. Details of the microscopic structure and the Ising Hamiltonian for the trilayer system are in Section II. In Section III, MCS scheme and the calculated quantities of interest are discussed, while details of the numerical results are in Section IV. Next, in Section V, there are concluding remarks, summary of the article is in Section VI and acknowledgments are in Section VII.

## II. Model and the Interaction Hamiltonian

We consider, in this study, an Ising superlattice containing three magnetic layers on square lattice structure with the following details (as in [22,23]):

- (a) Each layer is exhaustively composed by either of the two possible types of atoms, A or B with coordination number being 6 or 5 depending on that site being on the mid-layer or on the surface layers.
- (b) Three types of interactions exist:
  - A-A  $\rightarrow$  Ferromagnetic
  - B-B  $\rightarrow$  Ferromagnetic
  - A-B  $\rightarrow$  Anti-ferromagnetic
- (c) Two distinct stackings are possible: (i) AAB (Fig.-1a) and (ii) ABA (Fig.-1b).

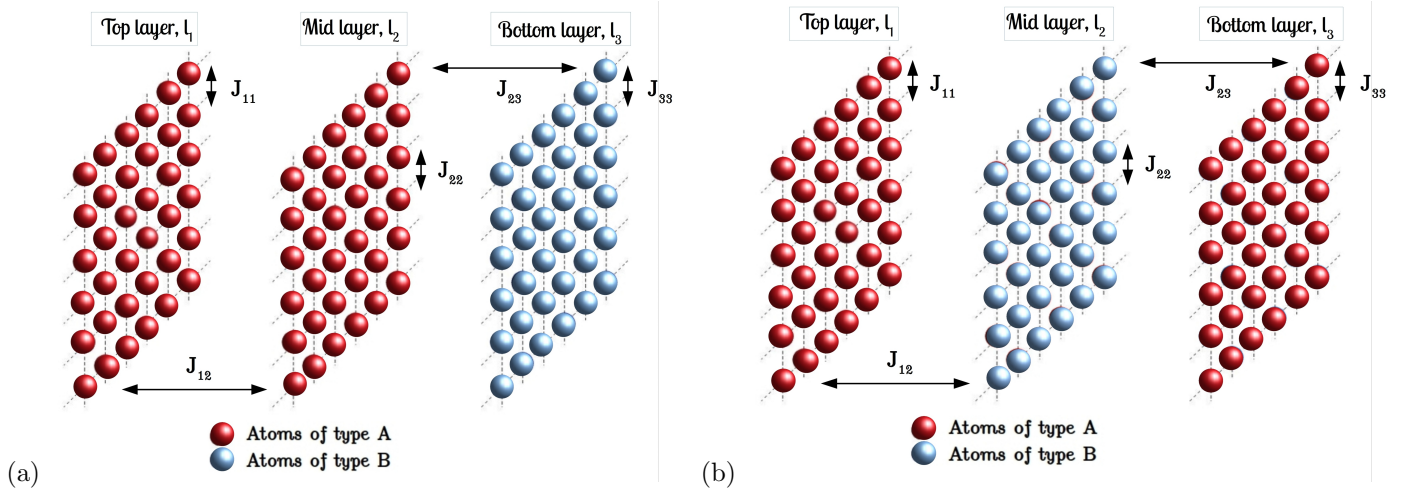


Figure 1: Two distinct trilayer stackings: (a) AAB stacking (with  $J_{11} = J_{22} = J_{12} = J_{AA}$ ,  $J_{33} = J_{BB}$  and  $J_{23} = J_{AB}$ )(b) ABA stacking (with  $J_{11} = J_{33} = J_{AA}$ ,  $J_{22} = J_{BB}$  and  $J_{12} = J_{23} = J_{AB}$ ).

The equilibrium spin configuration on any layer is determined by the condition that the free energy of the whole system should be a minimum. As we've considered the spins to interact Ising-like, in-plane as well as out-of-plane, the Hamiltonian for the trilayer system is:

$$H = -J_{11} \sum_{\langle t, t' \rangle} S_t S_{t'} - J_{22} \sum_{\langle m, m' \rangle} S_m S_{m'} - J_{33} \sum_{\langle b, b' \rangle} S_b S_{b'} - J_{12} \sum_{\langle t, m \rangle} S_t S_m - J_{23} \sum_{\langle m, b \rangle} S_m S_b \quad (1)$$

where summation indices  $(t, t')$ ,  $(m, m')$  and  $(b, b')$  denote respectively the lattice sites on the top-layer,  $l_1$ ; mid layer,  $l_2$  and bottom-layer,  $l_3$  and  $\langle t, t' \rangle$ ,  $\langle m, m' \rangle$ ,  $\langle b, b' \rangle$  are summations over all nearest-neighbor pairs in the same layer and  $\langle t, m \rangle$ ,  $\langle m, b \rangle$  are summations over pairs of nearest-neighbor sites in adjacent layers. In Equation (1), the first, second and third terms respectively are for the intra-planar ferromagnetic contributions from the top-layer, mid-layer and bottom-layer. The fourth and the fifth terms arise out of the nearest neighbour inter-planar antiferromagnetic interactions, between top and mid layers and mid and bottom layers.

For the ABA type trilayer system, the nature of the coupling strengths in Equation (1) are:  $J_{11} > 0$ ,  $J_{22} > 0$ ,

$J_{33} > 0$  and  $J_{12} < 0$ ,  $J_{23} < 0$  supporting ferromagnetic intraplanar and anti-ferromagnetic inter-planar interactions and we call  $J_{11} = J_{33} = J_{AA}$ ,  $J_{22} = J_{BB}$  and  $J_{12} = J_{23} = J_{AB}$ .

But when we switch to AAB type system, we have in Equation (1):  $J_{11} > 0$ ,  $J_{22} > 0$ ,  $J_{33} > 0$  and  $J_{12} > 0$ ,  $J_{23} < 0$  as the inter-layer interaction of top and mid layer is ferromagnetic and the rest remains similar to that of ABA system. and we call  $J_{11} = J_{22} = J_{12} = J_{AA}$ ,  $J_{33} = J_{BB}$  and  $J_{23} = J_{AB}$ . We've considered periodic boundary conditions in-plane and open boundary conditions along the vertical, so that there is no out-of-plane interaction term between the top and bottom layer in the Hamiltonian.

### III. Simulation scheme and calculated quantities

The model described above was simulated using the Monte Carlo simulations with Metropolis single spin-flip algorithm [17,18] with each plane having  $L^2$  sites with a system size having  $L = 100$ . The initial high temperature paramagnetic phase of spin configurations had randomly selected 50% of total number of spins in upward projection with  $S_i = +1$  and the rest in downward projection with  $S_i = -1$  (Using 1 instead of 1/2 rescales the coupling constants only). At a fixed temperature  $T$ , spin flipping from  $S_i$  to  $-S_i$  was done by using the Metropolis rate [17,18]:

$$P(S_i \rightarrow -S_i) = \min\{1, \exp(-\Delta E/k_B T)\} \quad (2)$$

where  $\Delta E$  is the change in internal energy due to the change of the orientation of the  $i$ -th spin projection from  $S_i$  to  $-S_i$  with Boltzmann constant,  $k_B$  to 1. Similar  $3L^2$  random updates of spins constitute one Monte Carlo sweep per spin (MCSS) and define one unit of time in our study. At each temperature step, starting from the configuration of previous temperature step, the system was equilibrated till  $5 \times 10^5$  MCSS (that is equivalent to allowance of a long enough *time*) and thermal averages were calculated from further  $5 \times 10^5$  MCSS. We observed the system for ten values of  $J_{AA}/J_{BB}$ , starting from 0.1 to 1.0 and for each fixed value of  $J_{AA}/J_{BB}$ , we varied  $J_{AB}/J_{BB}$  from 0.1 to 1.0 with an interval of 0.1. For each of the values of  $J_{AA}/J_{BB}$  and  $J_{AB}/J_{BB}$ , we've calculated the ensemble averages of the following quantities at each of the temperature points, after sample averaging over 10 statistically independent microscopic samples with same macroscopic initial conditions:

(1) **Sublattice magnetisations** for top, mid and bottom layers, denoted by  $M_t$ ,  $M_m$ ,  $M_b$  by:

$$M_q = \frac{1}{L^2} \sum_{x,y=1}^L \langle S_{x,y} \rangle \quad (3)$$

where  $q \in \{t, m, b\}$  and the sum extends over all sites in each of the planes as  $x$  and  $y$  denote the co-ordinates of a spin on a plane and runs from 1 to  $L = 100$ , after completion of one MCSS.  $\langle \dots \rangle$  denotes a time average after attaining equilibrium.

(2) **Average magnetisation of the trilayer** by  $M = \frac{1}{3} (M_t + M_m + M_b)$

(3) At equilibrium, we calculate **fluctuation in magnetisation**,  $\Delta M$  for each sample as follows (with  $N = TMCSS$ ):

$$\Delta M = \frac{2}{3NL^2} \sqrt{\sum_{i=\frac{N}{2}+1}^N (M_i - \langle M \rangle)^2} \quad (4)$$

where  $\langle M \rangle$  is the average value of magnetisation, calculated upon the last  $N/2$  MCSS (from  $\frac{N}{2} + 1$  to  $N$ ) and then make sample averages to report the values of these quantities.

From the plot of  $M$  vs. temperature, we find the values of compensation points by linear interpolation from immediate neighbouring points and reduced residual magnetisation and from the plot of  $\Delta M$  vs. temperature, we get the values of Neel temperatures and subsequently obtain the difference between Neel and compensation temperatures. After that we fit the obtained data so far to get the possible functional forms for these two quantities.

### IV. Results and Discussion

We have studied the thermodynamic and magnetic characteristics of a trilayer system along with its morphology for both types of stackings with MC simulation. Our goal is to observe the effects of Hamiltonian parameters on the critical temperature and the compensation temperature and finally obtain mathematical relationships for different related quantities.

From the plot of Fig.-2a, We first note the presence of compensation point, and note coordinates of immediate neighbouring points on both sides of zero line to find out the value of compensation point by the method of linear interpolation. Then, we find out the value of *residual magnetisation*, the intermediate maximum absolute value of magnetization between Néel temperature and saturated value and divide it by the value of magnetization at saturation and then call it *reduced residual magnetization*, which is a dimensionless quantity.

From the plot of Fig.-2b, We note the value of temperature where the fluctuation in magnetization reaches its maximum value, and quote that temperature as the critical temperature. All the while we would be working with best values of underlying quantities to qualitatively figure out mathematical dependences.

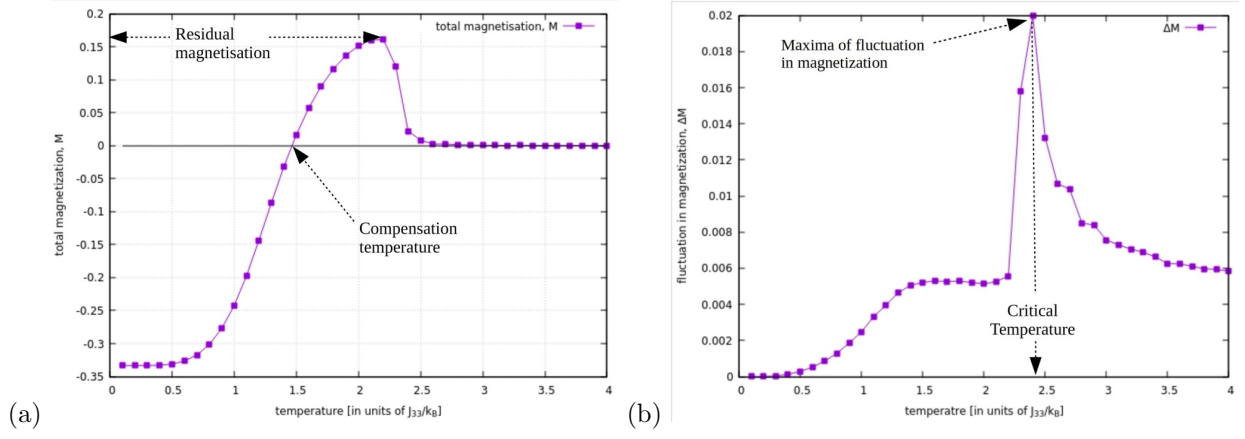


Figure 2: The plots of AAB configuration of (a) total magnetisation vs. temperature and (b) fluctuation in magnetization vs. temperature [for  $J_{AA}/J_{BB} = 0.3$  and  $J_{AB}/J_{BB} = -0.4$ ] show how observed quantities are extracted

### a. Morphology

In the study of morphology, we obtained the results for the systems in the presence of compensation effect. We show here the density plots of the spin matrices of three layers to show that the critical temperature and the compensation temperatures are morphologically different.

At  $T_{comp}$ , due to the configuration of AAB system, compensation happens for satisfying the following conditions (which can readily be verified from Fig.-3, Fig.-4 & Fig.-5):

$$|M_b| = |M_t + M_m| \quad (5)$$

$$\text{sgn}(M_b) = -\text{sgn}(M_t) \quad (6)$$

$$\text{sgn}(M_b) = -\text{sgn}(M_m) \quad (7)$$

Fig.-3, Fig.-4 and Fig.-5 are spin density matrix plots for AAB system with  $J_{AA}/J_{BB} = 0.3$  and  $J_{AB}/J_{BB} = -0.4$ . For an AAB system, the bottom-layer,  $b$ , is antiferromagnetically coupled to the mid-layer,  $m$  and thus magnetically saturates in the opposite direction to both,  $t$  and  $m$ . At  $T_{crit}$ , larger spin clusters results in bottom layer having greater absolute value of magnetisation than the top and mid layer.

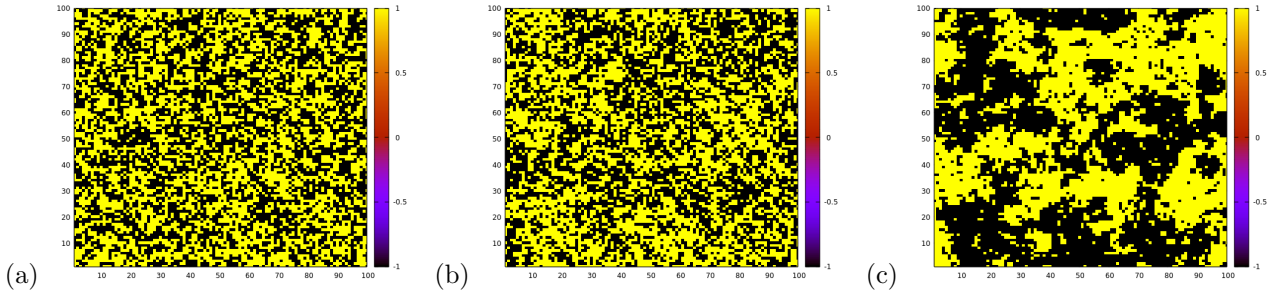


Figure 3: Morphology of (a) Top layer, (b) Mid layer and (c) Bottom layer for the AAB stacking ( $J_{AA}/J_{BB} = 0.3$  and  $J_{AB}/J_{BB} = -0.4$ ) at  $T_{crit} = 2.4$  with  $M_t = -0.01$ ,  $M_m = -0.05$ ,  $M_b = 0.17$ .

Similarly for ABA system, the conditions for compensation change to the following:

$$|M_m| = |M_t + M_b| \quad (8)$$

$$\text{sgn}(M_m) = -\text{sgn}(M_t) \quad (9)$$

$$\text{sgn}(M_m) = -\text{sgn}(M_b) \quad (10)$$

Fig.-6, Fig.-7, Fig.-8 are spin density matrix plots for ABA system with  $J_{AA}/J_{BB} = 0.3$  and  $J_{AB}/J_{BB} = -0.4$ . As the mid-layer,  $m$ , is antiferromagnetically coupled to both the  $t$  and  $b$  layers, mid-layer always magnetically saturates in the opposite direction to both,  $t$  and  $b$  layers for an ABA system. At  $T_{crit}$ , it is seen that larger spin clusters form in the mid layer resulting in its having greater absolute value of magnetisation than the top and bottom layer.

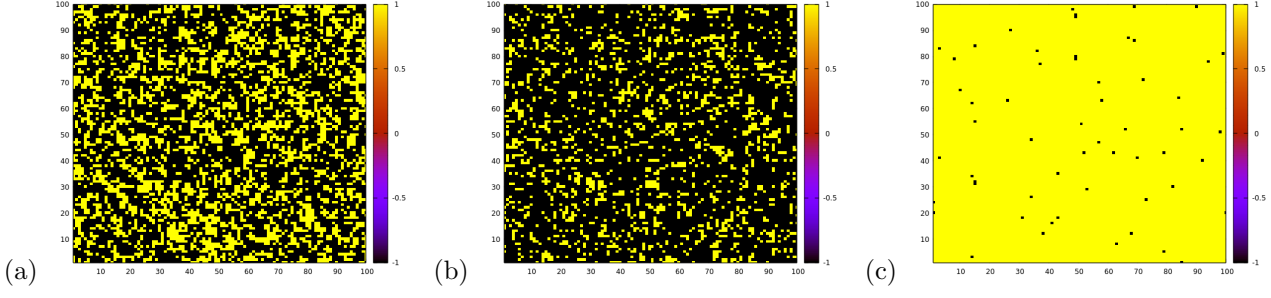


Figure 4: Morphology of (a) Top layer, (b) Mid layer and (c) Bottom layer for the AAB stacking ( $J_{AA}/J_{BB} = 0.3$  and  $J_{AB}/J_{BB} = -0.4$ ) at  $T = 1.5$  (immediate higher neighbour than  $T_{comp}$ ) with  $M_t = -0.32$ ,  $M_m = -0.62$ ,  $M_b = 0.99$ .

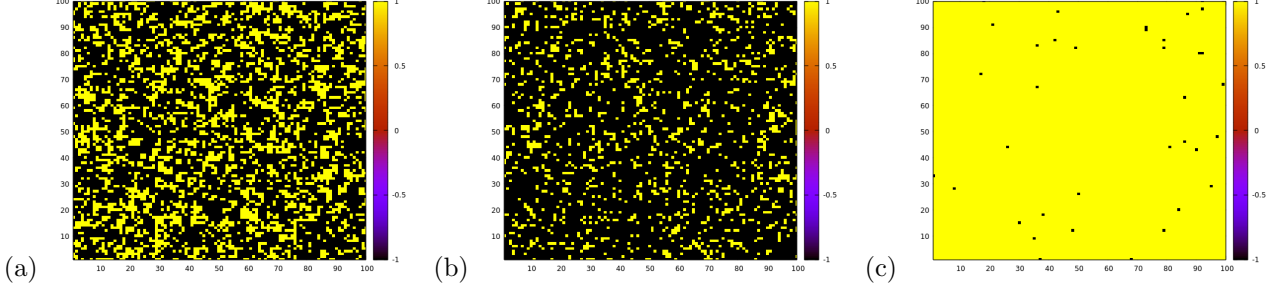


Figure 5: Morphology of (a) Top layer, (b) Mid layer and (c) Bottom layer for the AAB stacking ( $J_{AA}/J_{BB} = 0.3$  and  $J_{AB}/J_{BB} = -0.4$ ) at  $T = 1.4$  (immediate lower neighbour than  $T_{comp}$ ) with  $M_t = -0.39$ ,  $M_m = -0.69$ ,  $M_b = 0.99$ .

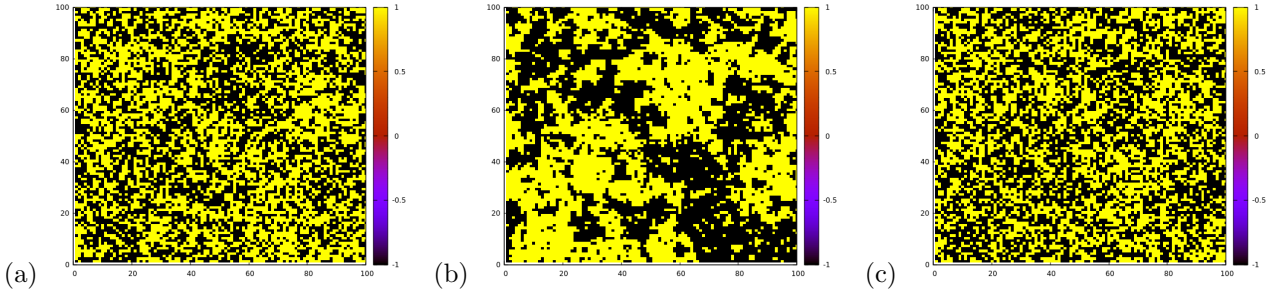


Figure 6: Morphology of (a) Top layer, (b) Mid layer and (c) Bottom layer for the ABA stacking ( $J_{AA}/J_{BB} = 0.3$  and  $J_{AB}/J_{BB} = -0.4$ ) at  $T_{crit} = 2.6$  with  $M_t = -2.91 \times 10^{-3}$ ,  $M_m = 1.23 \times 10^{-2}$ ,  $M_b = -3.07 \times 10^{-3}$ .

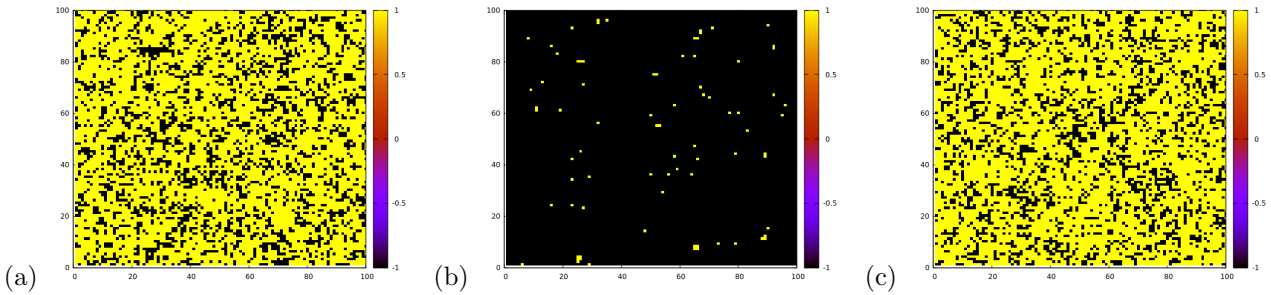


Figure 7: Morphology of (a) Top layer, (b) Mid layer and (c) Bottom layer for the ABA stacking ( $J_{AA}/J_{BB} = 0.3$  and  $J_{AB}/J_{BB} = -0.4$ ) at  $T = 1.7$ , (immediate higher neighbour than  $T_{comp}$ ) with  $M_t = -0.48$ ,  $M_m = 0.98$ ,  $M_b = -0.48$ .

## b. AAB composition

### Reduced Residual Magnetisation (RRM):

The behaviour of RRM with the variation of antiferromagnetic and ferromagnetic coupling strength ratios (AFM and FM ratios, for brevity)[Fig.-9] leads us to predict their behaviours in the following way: The plots of RRM vs. AFM

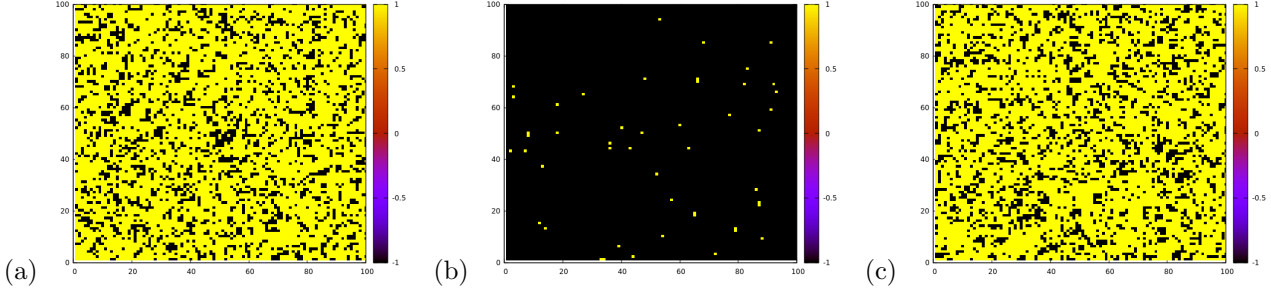


Figure 8: Morphology of (a) Top layer, (b) Mid layer and (c) Bottom layer for the ABA stacking ( $J_{AA}/J_{BB} = 0.3$  and  $J_{AB}/J_{BB} = -0.4$ ) at  $T = 1.6$  (immediate lower neighbour than  $T_{comp}$ ) with  $M_t = -0.53$ ,  $M_m = 0.99$ ,  $M_b = -0.53$ .

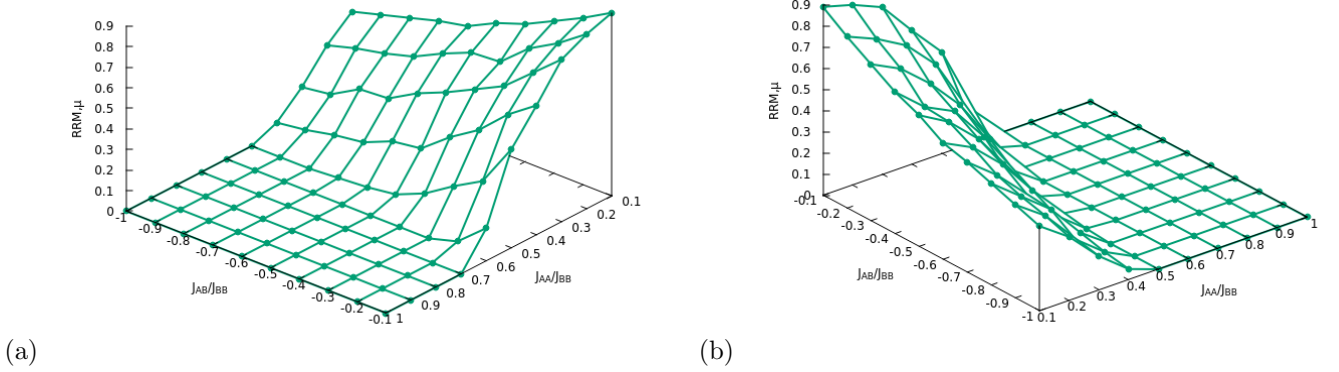


Figure 9: 3D plots of RRM vs. controlling factors for AAB configuration from two different angles of view.

ratio [Fig.-10a], for a fixed FM ratio, predicts a functional relationship,  $\Phi_1(J_{AA}/J_{BB}, J_{AB}/J_{BB})$ , like:

$$\Phi_1(J_{AA}/J_{BB}, J_{AB}/J_{BB}) = a_1 \exp \left[ -a_2 \left| \frac{J_{AB}}{J_{BB}} \right| \right] \quad (11)$$

where the coefficients  $a_1$  and  $a_2$  are functions of FM ratios i.e.  $a_1 \equiv a_1(J_{AA}/J_{BB})$  and  $a_2 \equiv a_2(J_{AA}/J_{BB})$  and Table 1 lists their variations.

$J_{AA}/J_{BB}$	0.1	0.2	0.3	0.4	0.5
$a_1$	$0.966 \pm 0.007$	$0.944 \pm 0.016$	$0.940 \pm 0.016$	$0.855 \pm 0.027$	$0.818 \pm 0.049$
$a_2$	$0.890 \pm 0.014$	$1.166 \pm 0.039$	$1.713 \pm 0.045$	$2.662 \pm 0.109$	$5.336 \pm 0.344$

Table 1: Variation of  $a_1$  and  $a_2$  with  $J_{AA}/J_{BB}$ , for AAB trilayer; the errors are standard asymptotic error for least square fitting

The plots of RRM vs. FM ratio [Fig.-10b], for fixed AFM ratios, predict a functional dependence,  $\Phi_2(J_{AA}/J_{BB}, J_{AB}/J_{BB})$ , like:

$$\Phi_2(J_{AA}/J_{BB}, J_{AB}/J_{BB}) = a_3 - a_4 \left( \frac{J_{AA}}{J_{BB}} \right)^2 \quad (12)$$

where the coefficients  $a_3$  and  $a_4$  are functions of  $J_{AB}/J_{BB}$  i.e.  $a_3 \equiv a_3(J_{AB}/J_{BB})$  and  $a_4 \equiv a_4(J_{AB}/J_{BB})$ . Variations of  $a_3$  and  $a_4$  are listed in Table 2:

#### Temperature gap between Critical and Compensation temperatures, $\Delta T$ :

The behaviour of temperature gap between Critical and Compensation temperatures with the variation of AFM and FM ratios [Fig.-11], leads us to predict its behaviour in similar fashion as before.

The plots of  $\Delta T$  vs. AFM ratio [Fig.-12a], for fixed FM ratios, predict a functional relationship,  $\Psi_1(J_{AA}/J_{BB}, J_{AB}/J_{BB})$ , like:

$$\Psi_1(J_{AA}/J_{BB}, J_{AB}/J_{BB}) = -a_5 \left| \frac{J_{AB}}{J_{BB}} \right| + a_6 \quad (13)$$

where the coefficients  $a_5$  and  $a_6$  are functions of FM ratios i.e.  $a_5 \equiv a_5(J_{AA}/J_{BB})$  and  $a_6 \equiv a_6(J_{AA}/J_{BB})$ . Changes in the values of  $a_5$  and  $a_6$  are listed in Table 3:



$J_{AB}/J_{BB}$	-0.1	-0.2	-0.3	-0.4	-0.5	-0.6	-0.7	-0.8	-0.9	-1.0
$a_3$	0.945 $\pm 0.027$	0.852 $\pm 0.017$	0.761 $\pm 0.003$	0.674 $\pm 0.016$	0.634 $\pm 0.020$	0.562 $\pm 0.014$	0.497 $\pm 0.016$	0.487 $\pm 0.031$	0.443 $\pm 0.030$	0.401 $\pm 0.026$
$a_4$	2.055 $\pm 0.138$	2.241 $\pm 0.088$	2.281 $\pm 0.022$	2.289 $\pm 0.118$	2.470 $\pm 0.140$	2.241 $\pm 0.101$	2.104 $\pm 0.241$	2.461 $\pm 0.168$	2.469 $\pm 0.320$	2.314 $\pm 0.279$

Table 2: Variation of  $a_3$  and  $a_4$  with  $J_{AB}/J_{BB}$ , for AAB trilayer; the errors are standard asymptotic errors for least square fitting

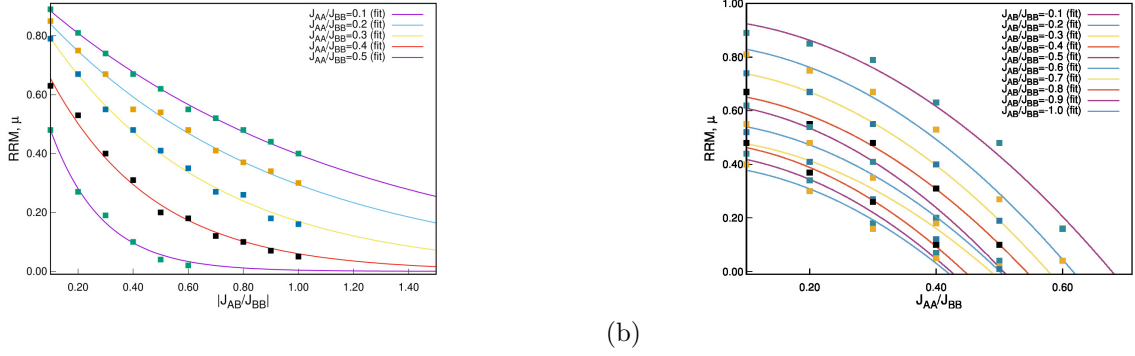


Figure 10: Plots of (a)  $\Phi_1$  vs.  $\left| \frac{J_{AB}}{J_{BB}} \right|$  (b)  $\Phi_2$  vs.  $\frac{J_{AA}}{J_{BB}}$  to show probable dependence of RRM of an AAB configuration.

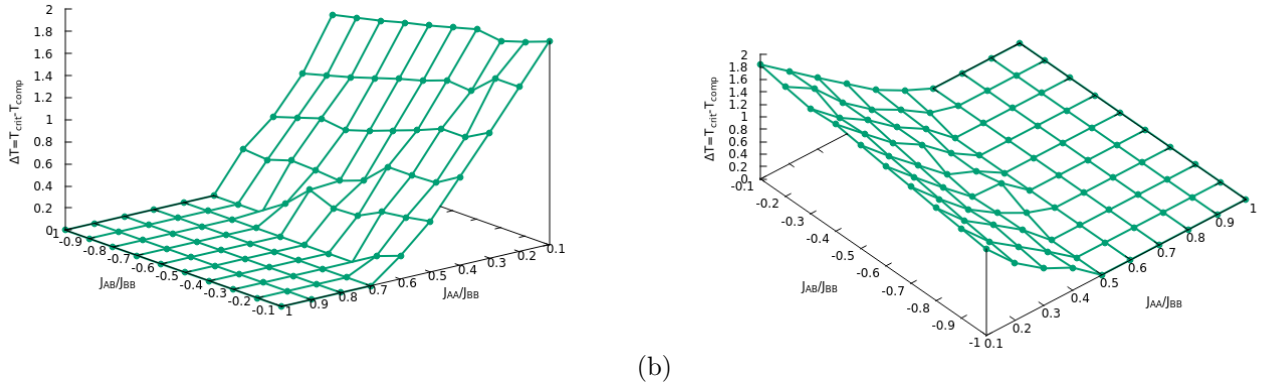


Figure 11: 3D plots of  $\Delta T = T_{crit} - T_{comp}$  vs. controlling factors for AAB configuration from two different angles of view.

$J_{AA}/J_{BB}$	0.1	0.2	0.3	0.4	0.5
$a_5$	$0.476 \pm 0.026$	$0.648 \pm 0.036$	$0.587 \pm 0.039$	$0.508 \pm 0.072$	$0.407 \pm 0.113$
$a_6$	$1.876 \pm 0.016$	$1.563 \pm 0.022$	$1.164 \pm 0.024$	$0.793 \pm 0.044$	$0.497 \pm 0.051$

Table 3: Variation of  $a_5$  and  $a_6$  with FM ratio, for AAB trilayer; the errors are standard asymptotic error for least square fitting

The plots of  $\Delta T$  vs. FM ratio [Fig.-12b], for fixed AFM ratios, predict a functional dependence,  $\Psi_2(J_{AA}/J_{BB}, J_{AB}/J_{BB})$ , like:

$$\Psi_2(J_{AA}/J_{BB}, J_{AB}/J_{BB}) = -a_7 \left( \frac{J_{AA}}{J_{BB}} \right) + a_8 \quad (14)$$

where the coefficients  $a_7$  and  $a_8$  are functions of  $J_{AB}/J_{BB}$  i.e.  $a_7 \equiv a_7(J_{AB}/J_{BB})$  and  $a_8 \equiv a_8(J_{AB}/J_{BB})$ . Variations of  $a_7$  and  $a_8$  are to be found in Table 4:

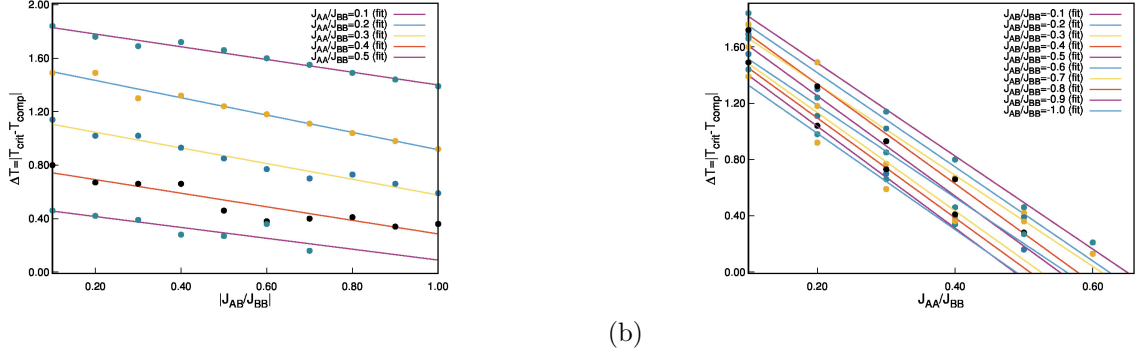


Figure 12: Plots of (a)  $\Psi_1$  vs.  $\left| \frac{J_{AB}}{J_{BB}} \right|$  (b)  $\Psi_2$  vs.  $\frac{J_{AA}}{J_{BB}}$  to show probable dependence of  $\Delta T$  of an AAB configuration.

$J_{AB}/J_{BB}$	-0.1	-0.2	-0.3	-0.4	-0.5	-0.6	-0.7	-0.8	-0.9	-1.0
$a_7$	3.308 $\pm 0.082$	3.346 $\pm 0.160$	3.240 $\pm 0.111$	3.540 $\pm 0.128$	3.560 $\pm 0.250$	3.280 $\pm 0.457$	3.490 $\pm 0.251$	3.550 $\pm 0.231$	3.620 $\pm 0.242$	3.420 $\pm 0.380$
$a_8$	2.148 $\pm 0.032$	2.086 $\pm 0.062$	1.984 $\pm 0.037$	2.044 $\pm 0.042$	1.964 $\pm 0.083$	1.842 $\pm 0.152$	1.831 $\pm 0.083$	1.805 $\pm 0.063$	1.760 $\pm 0.066$	1.670 $\pm 0.104$

Table 4: Variation of  $a_7$  and  $a_8$  with AFM ratio, for AAB trilayer; the errors are standard asymptotic errors for least square fitting

### c. ABA composition

#### Reduced Residual Magnetisation (RRM):

Observing the trends from the plots of RRM [Fig.-13, Fig.-14a, Fig.-14b], for the ABA configuration, like the AAB configuration we predict two functional relationships like,  $\Phi_3(J_{AA}/J_{BB}, J_{AB}/J_{BB})$  and  $\Phi_4(J_{AA}/J_{BB}, J_{AB}/J_{BB})$  as:

$$\Phi_3(J_{AA}/J_{BB}, J_{AB}/J_{BB}) = b_1 \exp \left[ -b_2 \left( \frac{J_{AB}}{J_{BB}} \right)^2 \right] \quad (15)$$

$$\Phi_4(J_{AA}/J_{BB}, J_{AB}/J_{BB}) = b_3 - b_4 \left( \frac{J_{AA}}{J_{BB}} \right)^2 \quad (16)$$

where the coefficients  $b_1$  and  $b_2$  are functions of FM ratios i.e.  $b_1 \equiv b_1(J_{AA}/J_{BB})$  and  $b_2 \equiv b_2(J_{AA}/J_{BB})$  and their

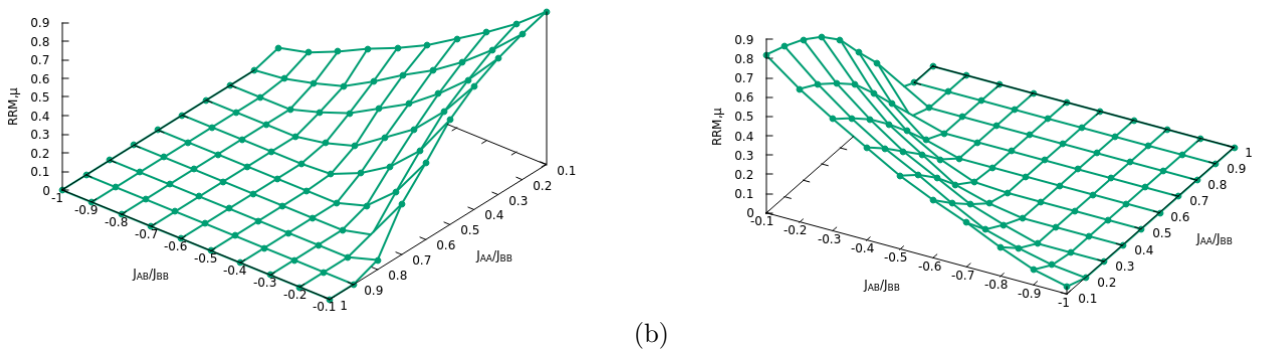


Figure 13: 3D plots of RRM vs. controlling factors for ABA configuration from two different angles of view.

variations are in Table 5 and the coefficients  $b_3$  and  $b_4$  are functions of AFM ratios i.e.  $b_3 \equiv b_3(J_{AB}/J_{BB})$  and  $b_4 \equiv b_4(J_{AB}/J_{BB})$  and their variations are in Table 6.

**Temperature gap between Critical and Compensation temperatures,  $\Delta T$  :**



$J_{AA}/J_{BB}$	0.1	0.2	0.3	0.4	0.5
$b_1$	$0.791 \pm 0.020$	$0.770 \pm 0.020$	$0.733 \pm 0.026$	$0.699 \pm 0.024$	$0.635 \pm 0.026$
$b_2$	$2.804 \pm 0.155$	$4.048 \pm 0.229$	$5.722 \pm 0.430$	$8.972 \pm 0.611$	$14.554 \pm 1.14$

Table 5: Variation of  $b_1$  and  $b_2$  with  $J_{AA}/J_{BB}$ , for ABA trilayer; the errors are standard asymptotic error for least square fitting

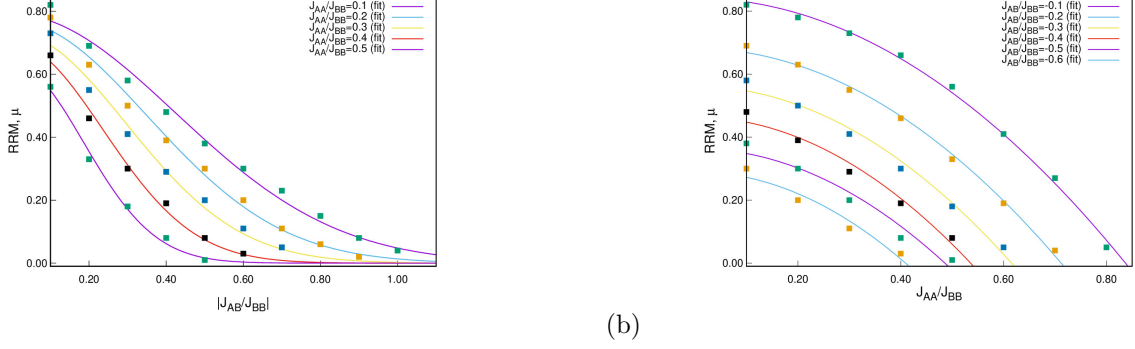


Figure 14: Plots of (a)  $\Phi_3$  vs.  $\left| \frac{J_{AB}}{J_{BB}} \right|$  (b)  $\Phi_4$  vs.  $\frac{J_{AA}}{J_{BB}}$  to show probable dependence of  $\Delta T$  of an ABA configuration.

$J_{AB}/J_{BB}$	-0.1	-0.2	-0.3	-0.4	-0.5	-0.6
$b_3$	$0.841 \pm 0.009$	$0.682 \pm 0.009$	$0.562 \pm 0.017$	$0.464 \pm 0.021$	$0.363 \pm 0.026$	$0.290 \pm 0.026$
$b_4$	$1.201 \pm 0.027$	$1.345 \pm 0.036$	$1.482 \pm 0.086$	$1.615 \pm 0.152$	$1.540 \pm 0.189$	$1.729 \pm 0.282$

Table 6: Variation of  $b_3$  and  $b_4$  with  $J_{AB}/J_{BB}$ , for ABA trilayer; the errors are standard asymptotic error for least square fitting

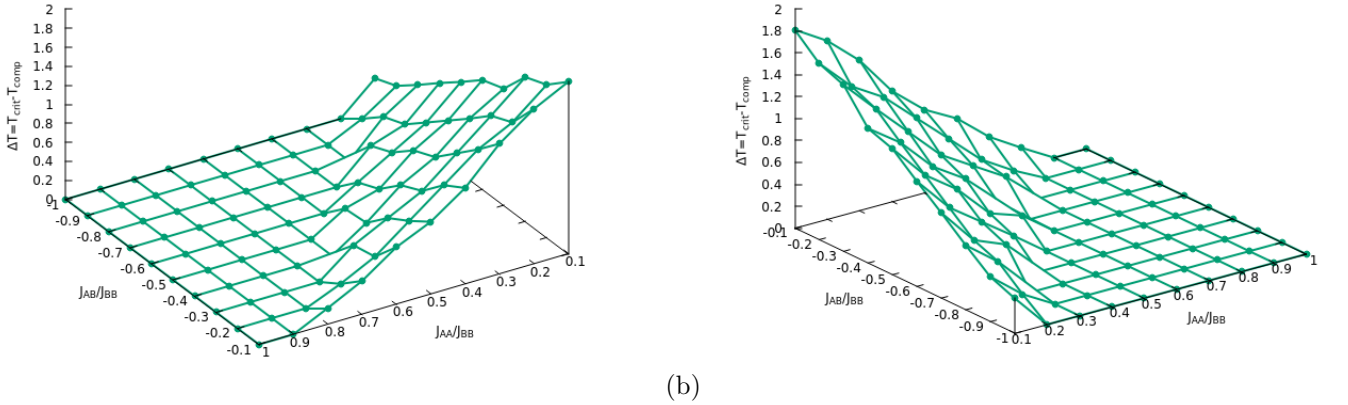


Figure 15: 3D plots of  $\Delta T$  vs. controlling factors for ABA configuration from two different angles of view.

The plots of  $\Delta T$  [Fig.-15, Fig.-16a, Fig.-16b] predict functional relationships like:

$$\Psi_3(J_{AA}/J_{BB}, J_{AB}/J_{BB}) = -b_5 \left| \frac{J_{AB}}{J_{BB}} \right| + b_6 \quad (17)$$

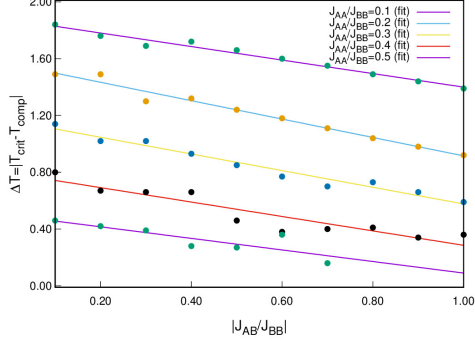
$$\Psi_4(J_{AA}/J_{BB}, J_{AB}/J_{BB}) = -b_7 \left( \frac{J_{AA}}{J_{BB}} \right) + b_8 \quad (18)$$

where  $b_5 \equiv b_5(J_{AA}/J_{BB})$ ;  $b_6 \equiv b_6(J_{AA}/J_{BB})$  and  $b_7 \equiv b_7(J_{AB}/J_{BB})$ ;  $b_8 \equiv b_8(J_{AB}/J_{BB})$ .

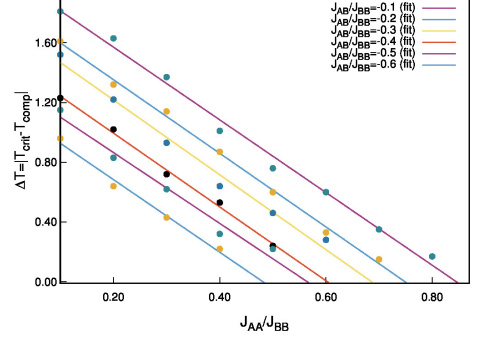
The obtained data of  $b_5$  and  $b_6$ , are in Table 7. Refer to Table 8 for the variations of  $b_7$  and  $b_8$ .

$J_{AA}/J_{BB}$	0.1	0.2	0.3	0.4	0.5
$b_5$	$0.476 \pm 0.026$	$0.648 \pm 0.036$	$0.587 \pm 0.039$	$0.508 \pm 0.072$	$0.407 \pm 0.113$
$b_6$	$1.876 \pm 0.016$	$1.563 \pm 0.022$	$1.164 \pm 0.024$	$0.793 \pm 0.045$	$0.497 \pm 0.051$

Table 7: Variation of  $b_5$  and  $b_6$  with  $J_{AA}/J_{BB}$ , for ABA trilayer; the errors are standard asymptotic error for least square fitting



(a)



(b)

Figure 16: Plots of (a)  $\Psi_3$  vs.  $\left| \frac{J_{AB}}{J_{BB}} \right|$  (b)  $\Psi_4$  vs.  $\frac{J_{AA}}{J_{BB}}$  to show probable dependence of  $\Delta T$  of an ABA configuration.

$J_{AB}/J_{BB}$	-0.1	-0.2	-0.3	-0.4	-0.5	-0.6
$b_7$	$2.433 \pm 0.091$	$2.464 \pm 0.059$	$2.506 \pm 0.142$	$2.470 \pm 0.093$	$2.370 \pm 0.208$	$2.430 \pm 0.190$
$b_8$	$2.056 \pm 0.046$	$1.846 \pm 0.026$	$1.719 \pm 0.055$	$1.489 \pm 0.031$	$1.339 \pm 0.069$	$1.170 \pm 0.052$

Table 8: Variation of  $b_7$  and  $b_8$  with  $J_{AB}/J_{BB}$ , for ABA trilayer; the errors are standard asymptotic errors for least square fitting

## V. Conclusion

### a. AAB composition:

The zeroes of the function  $\Phi_2$  lead us to the specific combinations of the coupling ratios for AAB composition Table 9 where the compensation ceases to exist within the ranges of our observation.

$J_{AB}/J_{BB}$	-0.1	-0.2	-0.3	-0.4	-0.5	-0.6	-0.7	-0.8	-0.9	-1.0
$J_{AA}/J_{BB}$	0.678	0.616	0.578	0.543	0.507	0.501	0.486	0.445	0.424	0.416
	$\pm 0.008$	$\pm 0.014$	$\pm 0.017$	$\pm 0.021$	$\pm 0.024$	$\pm 0.024$	$\pm 0.038$	$\pm 0.025$	$\pm 0.035$	$\pm 0.034$

Table 9: Table for maximum values of  $J_{AA}/J_{BB}$  for a fixed  $J_{AB}/J_{BB}$  for which the compensation effect just ceases, from the fitted formula of variation of RRM

Similarly We use zeroes of the function  $\Psi_2$  to determine another set of specific combinations of the coupling ratios Table 10 for AAB configuration where the compensation just ceases to exist, from the data of temperature difference of  $T_{crit}$  and  $T_{comp}$ .

$J_{AB}/J_{BB}$	-0.1	-0.2	-0.3	-0.4	-0.5	-0.6	-0.7	-0.8	-0.9	-1.0
$J_{AA}/J_{BB}$	0.649	0.623	0.612	0.577	0.552	0.562	0.525	0.508	0.486	0.488
	$\pm 0.019$	$\pm 0.035$	$\pm 0.024$	$\pm 0.024$	$\pm 0.045$	$\pm 0.091$	$\pm 0.045$	$\pm 0.038$	$\pm 0.037$	$\pm 0.062$

Table 10: Maximum values of  $J_{AA}/J_{BB}$  for fixed  $J_{AB}/J_{BB}$  for which the compensation effect just ceases, from the fitted formula of  $\Psi_2$

We can finally write the fitted formulae [Equation (19) and Equation (20)] for RRM (say,  $\mu$ ) and  $\Delta T$  for AAB configuration as:

$$\left| \frac{M_{max,int}}{M_{sat}} \right| = \mu \left( \frac{J_{AA}}{J_{BB}}, \frac{J_{AB}}{J_{BB}} \right) = a_1 e^{-a_2 |J_{AB}/J_{BB}|} \left[ a_3 - a_4 \left( \frac{J_{AA}}{J_{BB}} \right)^2 \right] \quad (19)$$

$$T_{crit} - T_{comp} = \Delta T \left( \frac{J_{AA}}{J_{BB}}, \frac{J_{AB}}{J_{BB}} \right) = \left[ -a_5 \left| \frac{J_{AB}}{J_{BB}} \right| + a_6 \right] \left[ -a_7 \left( \frac{J_{AA}}{J_{BB}} \right) + a_8 \right] \quad (20)$$

The coefficients  $a_1, a_2, a_3, a_4, a_5, a_6, a_7$  and  $a_8$  all are functions of  $\frac{J_{AA}}{J_{BB}}$  and  $\frac{J_{AB}}{J_{BB}}$ .

### b. ABA composition:

The zeroes of the function  $\Phi_4$  lead us to determine the specific combination of the coupling ratios from the RRM data for ABA composition where the compensation just ceases to exist (Table 11).

$J_{AB}/J_{BB}$	-0.1	-0.2	-0.3	-0.4	-0.5	-0.6
$J_{AA}/J_{BB}$	$0.837 \pm 0.010$	$0.712 \pm 0.011$	$0.616 \pm 0.020$	$0.536 \pm 0.028$	$0.486 \pm 0.035$	$0.410 \pm 0.038$

Table 11: Table for maximum values of  $J_{AA}/J_{BB}$  for a fixed  $J_{AB}/J_{BB}$  for which the compensation effect just ceases, from the fitted formula of variation of RRM

Similarly zeroes of  $\Psi_4$  lead us to the combinations of the coupling ratios from the  $\Delta T$  data for ABA composition where the compensation just ceases to exist (Table 12). We can finally write the fitted formulae [Equation (21)

$J_{AB}/J_{BB}$	-0.1	-0.2	-0.3	-0.4	-0.5	-0.6
$J_{AA}/J_{BB}$	$0.845 \pm 0.037$	$0.749 \pm 0.021$	$0.686 \pm 0.045$	$0.603 \pm 0.026$	$0.565 \pm 0.058$	$0.481 \pm 0.043$

Table 12: Maximum values of  $J_{AA}/J_{BB}$  for a fixed  $J_{AB}/J_{BB}$  for which the compensation effect just ceases, from the fitted formula of variation of  $\Delta T$

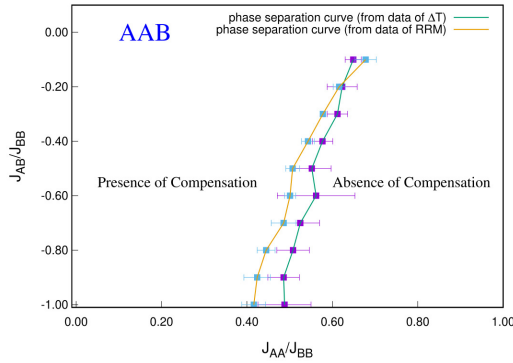
and Equation (22)] for RRM (say,  $\mu$ ) and  $\Delta T$  for ABA configuration as:

$$\left| \frac{M_{max,int}}{M_{sat}} \right| = \mu \left( \frac{J_{AA}}{J_{BB}}, \frac{J_{AB}}{J_{BB}} \right) = b_1 e^{-b_2 (J_{AB}/J_{BB})^2} \left[ b_3 - b_4 \left( \frac{J_{AA}}{J_{BB}} \right)^2 \right] \quad (21)$$

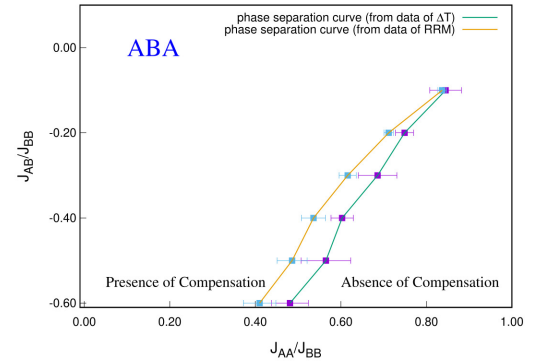
$$T_{crit} - T_{comp} = \Delta T \left( \frac{J_{AA}}{J_{BB}}, \frac{J_{AB}}{J_{BB}} \right) = \left[ -b_5 \left| \frac{J_{AB}}{J_{BB}} \right| + b_6 \right] \left[ -b_7 \left( \frac{J_{AA}}{J_{BB}} \right) + b_8 \right] \quad (22)$$

The coefficients  $b_1, b_2, b_3, b_4, b_5, b_6, b_7$  and  $b_8$  all are functions of  $\frac{J_{AA}}{J_{BB}}$  and  $\frac{J_{AB}}{J_{BB}}$ .

Fig.-17 shows the phase separation curves obtained for two types of configurations under our valid ranges of observations which agree fairly well with [23] where the curves are obtained via MFA, EFA and MC simulations.



(a)



(b)

Figure 17: Phase diagrams of (a) AAB and (b) ABA configurations from the fitted formulae; in both of the figures: rightside of the curves denote ferrimagnetic phase without compensation and left of the curves denote ferrimagnetic phase with compensation.

## VI. Summary

Summarising, we have simulated magnetic and thermodynamic properties of a spin-1/2 Ising trilayer system on square lattice. The three planes of the system is made up of only one type of atoms, out of two i.e. A or B. The interactions between same type of atoms (A-A or B-B bonds) are ferromagnetic and between dissimilar atoms (A-B) is antiferromagnetic. We have presented our results, obtained via Monte Carlo simulation with single spin flip algorithm, analysed with the help of linear interpolation, and linear, quadratic and exponential curve fitting techniques.

We have shown variations of reduced residual magnetisation and temperature gap between critical and compensation temperatures for a range of values of the Hamiltonian parameters and have proposed formulae for the mentioned quantities. The dynamics governed by these formulae leads to the phase diagrams ( $J_{AB}/J_{BB}$  vs.  $J_{AA}/J_{BB}$ ) for both AAB and ABA type systems, which clearly divides the controlling parameter space into two regions: one with compensation and the other without compensation. In the phase diagrams where there is compensation, we clearly see that the range of  $J_{AA}/J_{BB}$  increases as  $|J_{AB}/J_{BB}|$  gets smaller and the compensation happens only when  $J_{AA} < J_{BB}$  which is in fair agreement with [23] and supports the findings in [22,40,41] for similar systems made up of antiferromagnetic and ferromagnetic bonds. It would be interesting to study the behaviours of residual magnetisation and the difference in the critical and compensation temperature in the case of mixed spin [42, 43] system.

## VII. Acknowledgements

S.C. and M.A. would thank respectively University Grants Commission (for providing him fellowship through JRF in Science, Humanities & Social Sciences) and FRPDF grant of Presidency University for financial assistance. S.C. would like to extend his thanks to his doctoral colleague Tamaghna Maitra for helping him in different needs in this study.

## References

1. von E. Warburg, Ann. Phys. **249(5)** (1881) 141.
2. Debye P., Ann. Phys. **386** (1926) 1154.
3. Giaque W.F., J. Am. Chem. Soc. **49** (1927) 1864.
4. Spichkin Y I and Tishin A M, *The Magnetocaloric Effect and Its Applications* (Institute of Physics Publishing, Philadelphia, 2003).
5. Tishin A and Spichkin Y, Int. J. Refrigeration **37** (2014) 223 .
6. Gschneidner K A Jr, Pecharsky V K and Tsokol A O, Rep. Prog. Phys. **68** (2005) 1479 .
7. Szymczak H and Szymczak R, Mater. Sci. Poland **26** (2008), 807.
8. Topilko M, Krokhmalkii T, Derzhko O and Ohanyan V, Eur. Phys. J. B **85** (2012) 278.
9. Trippe C, Honecker A, Klümper A and Ohanyan V, Phys. Rev. B **81** (2010) 054402.
10. Pełka R et al., Acta Phys. Pol. A **124** (2013) 977.
11. Franco V, Conde A, Romero-Enrique J M and Blázquez J S, J. Phys.: Condensed Matter **20** (2008) 285207.
12. Amaral J S and Amaral V S, **Chapter 8** in *Thermodynamics: Systems in Equilibrium and Non-Equilibrium*, edited by J C Moreno-Piraján, pp. 173-198 (2011).
13. Amaral J S, Silva N J O and Amaral V S, Appl. Phys. Lett. **91** (2007) 172503.
14. de Oliveira N and von Ranke P, Phys. Rep. **489** (2010) 89.
15. Dong Q Y, Zhang H W, Sun J R, Shen B G and Franco V, J. Appl. Phys. **103** (2008) 116101.
16. Basso V, Sasso C P and Küpferling M, Int. J. Refrigeration **37** (2014) 257.
17. K. Binder, D.W. Heermann, *Monte Carlo simulation in Statistical Physics* (Springer, New York, 1997).
18. M.E.J. Newman, G.T. Barkema, *Monte Carlo methods in Statistical Physics* (Oxford University Press, New York, 1999)
19. Nóbrega E P, de Oliveira N A, von Ranke P J and Troper A, Phys. Rev. B **72** (2005) 134426.

20. Nóbrega E P, de Oliveira N A, von Ranke P J and Troper A, J. Magn. Magn. Mater. **310** (2007) 2805.
21. Singh N and Arróyave R, J. Appl. Phys. **113** (2013) 183904.
22. I.J.L. Diaz and N.S. Branco, Physica B **73** (2017) 529.
23. I.J.L. Diaz and N.S. Branco, Physica A **540** (2019) 123014.
24. Connell G, Allen R, Mansuripur M., J. Appl. Phys. **53** (1982) 7759.
25. H. P. D. Shieh and M. H. Kryder, Applied physics letters **49** (1986) 473.
26. J. Ostorero, M. Escorne, A. Pecheron-Guegan, F. Soulette, and H. Le Gall, Journal of Applied Physics **75** (1994) 6103.
27. Sk Sajid and M. Acharyya, Phase Transitions **93** (2020) 62.
28. S. Chandra and M. Acharyya, AIP Conference Proceedings **2220** (2020) 130037.
29. M. Stier and W. Nolting, Phys. Rev. B **84** (2011) 094417.
30. C.J.P. Smits, A.T. Filip, H.J.M. Swagten, et. al., Phys. Rev. B **69** (2004) 224410.
31. J. Leiner, H. Lee, T. Yoo, et. al., Phys. Rev. B **82** (2010) 195205.
32. H. Kepa, J. Kutner-Pielaszek and J. Blinowski, Eur. Phys. Lett. **56** (2001) 54.
33. G. Chern, L. Horng and W.K. Sheih, Phys. Rev. B **63** (2001) 094421.
34. P. Sankowski and P. Kacmann, Phys. Rev. B **71** (2005) 201303(R).
35. J.H. Chung, Y.S. Song and T. Yoo, J. Appl. Phys. **110** (2011) 013912.
36. Z. Fadil, M. Qajjour, A. Mhirech, Physica B. **564** (2019) 104.
37. Z. Fadil, A. Mhirech, B. Kabouchi, Superlattice Microst. **134** (2019) 106224.
38. Z. Fadil, M. Qajjour, A. Mhirech, J Magn Magn Mater. **491** (2019) 165559.
39. M. Acharyya, arXiv:2004.03930 (2020).
40. T. Balcerzak, K. Szałowski, Physica A **395** (2014) 183.
41. K. Szałowski, T. Balcerzak, J. Phys.: Condensed Matter **26** (2014) 386003.
42. J D Alzate-Cardona, M C Barrero-Moreno and E Restrepo-Parra, J. Phys: Cond. Mat. **29** (2017) 445801
43. J.D. Alzate-Cardona, D. Sabogal-Suarez and E. Restrepo-Parra, J. Magn. Magn. Mater. **429** (2017) 34